doi:10.1017/S1431927615013100

Dynamics in Electrostatic Repetitive Systems via High-Order Transfer Maps

Kyoko Makino and Martin Berz

Department of Physics and Astronomy, Michigan State University, East Lansing, Michigan, USA

Traditionally most large storage rings for nuclear and high energy physics use magnetic particle optical elements for focusing and bending. However, recent interest in the study of the possible existence of an electric dipole moment (EDM) of protons, deuterons and others [1, 2] require the use of electrostatic elements in rings, and would even greatly benefit from the use of purely electrostatic lattices without any magnetic elements. Indeed the classical Thomas-BMT equation describing the motion of the spin due to a magnetic dipole moment coupling to magnetic fields can be augmented to analogously also describe the effects of a possibly present electric dipole moment coupling to electric fields, and the additional term would lead to detectable effects.

We discuss how to address and resolve various particle optical problems appearing in the simulation of such lattices. We begin with methods that allow the computation of all aberrations of individual elements to high orders, typically up to order seven or nine, including the fringe fields of the elements. We also discuss a problem arising in these rings, namely the possible non-conservation of the particle energies.

Dynamics in particle optics is usually expressed in terms of curvilinear coordinates [3] in which an orthogonal coordinate system $\{s,x,y\}$ is attached to the reference particle, which is denoted by the subscript 0; s is the position along the reference orbit, and, x and y are the horizontal and the vertical directions. Define $a = p_x/p_0$, $b = p_y/p_0$, $l = (t-t_0)\kappa$, $\delta = (K-K_0)/K_0$, where $\kappa = -v_0\gamma_0/(1+\gamma_0)$ and K is the kinetic energy. The variables in the optical coordinates $\vec{Z} = (x,a,y,b,l,\delta)$ form three canonically conjugate pairs, and we arrive at the following equations of motion:

$$x' = a(1+hx)\frac{p_0}{p_s}, \quad a' = (1+hx)\left(\frac{1+\eta}{1+\eta_0}\frac{p_0}{p_s}\frac{E_x}{\chi_{e0}} - \frac{B_y}{\chi_{m0}} + b\frac{p_0}{p_s}\frac{B_s}{\chi_{m0}}\right) + h\frac{p_s}{p_0}, \qquad \delta' = 0,$$

$$y' = b(1+hx)\frac{p_0}{p_s}, \quad b' = (1+hx)\left(\frac{1+\eta}{1+\eta_0}\frac{p_0}{p_s}\frac{E_y}{\chi_{e0}} + \frac{B_x}{\chi_{m0}} - a\frac{p_0}{p_s}\frac{B_s}{\chi_{m0}}\right), \qquad l' = \left[(1+hx)\frac{1+\eta}{1+\eta_0}\frac{p_0}{p_s} - 1\right]\frac{\kappa}{v_0}.$$

Here h is the curvature of the reference orbit, $\eta = [K_0(1+\delta) - ZeV]/mc^2$ is a relativistic measure, and $\chi_e = pv/Ze$ and $\chi_m = p/Ze$ are the electric and the magnetic rigidities which describe the strengths of coupling to the electric and magnetic fields.

When comparing χ_e and χ_m in SI units, we observe that because of the additional factor v, the electric rigidity is around eight orders of magnitude larger for relativistic particles. Considering that magnets easily reach strengths of 1 T and the superconducting bending magnets at the LHC are operated at ~ 8 T, this quickly shows that to achieve bending similar to the magnetic case requires electric fields in the neighborhood of 10^9 V/m. Yet actual practically achievable limits are a few tens of MV/m, which are also the fields achievable in the Van de Graaff generator and incidentally also those found in lightning. This is the reason that electrostatic elements are limited to moderate energies, and their desired use in storage ring EDM studies represents a new frontier of their use.

Once the fields are known, the equations of motion determine the final status of the coordinate variables $\vec{Z}_f$ depending on the initial status $\vec{Z}_i$. Except for simplified models of electromagnetic elements, one may

resort to numerical integrations of the differential equations on computers to relate $\vec{Z}_f$ and $\vec{Z}_i$. However, using the Differential Algebraic (DA) method [4] one can readily obtain the transfer map $\mathscr{M}$ relating final conditions to initial conditions via $\vec{Z}_f = \mathscr{M}(\vec{Z}_i)$, where the order is limited only by computer resources. But the use of DA methods is not limited to transfer maps, it allows the development of numerous other interesting and useful computational algorithms. In fact, some DA-based algorithms can be used to efficiently handle the field description for the equations of motion. In fact, the DA PDE solver [4, 5] is the main mechanism to supply the 3D fields including the derivatives at any position along the transfer map flow integration for nontrivial electromagnetic elements in the code COSY INFINITY [6], freeing the code from the need to rely on the conventional field computation methods such as FEM and BEM as well as subsequent numerical interpolation and numerical differentiation. As we see below, also repetitive tracking greatly benefits from the DA method since the transfer map has to be computed for only one revolution, resulting in significant speed gains in tracking [7, 8].

Using a general form of the Laplace equation [9, 10, 11] expressed in curvilinear coordinates, we outline the principle of the DA PDE solver. First, we bring the equation into a fixed point form:

$$V = V|_{y=0} + \int_0^y \frac{1}{b_2}\left(b_2\frac{\partial V}{\partial y}\right)\Big|_{y=0} - \int_0^y \frac{1}{b_2}\int_0^y \left(\frac{a_1}{b_1}\frac{\partial}{\partial x}\left(a_2\frac{\partial V}{\partial x}\right) + \frac{c_1}{b_1}\frac{\partial}{\partial z}\left(c_2\frac{\partial V}{\partial z}\right)\right) dydy,$$

where a_i, b_i, c_i are functions of x, y, z. Viewing it as a DA fixed point problem, we provide the boundary conditions $V|_{y=0}$ and $(b_2 \cdot \partial V/\partial y)|_{y=0}$ as DA quantities, that is the field description in the midplane as analytical functions of x and z. Then the right hand side is contracting with respect to y in the DA framework [4], and we obtain V as a function of x, y, z by calculating the equation in the DA arithmetic iteratively in finitely many steps.

For the main fields of an electromagnetic element, one carefully attempts to keep the field constant along the reference trajectory. However, in the fringe field region, unavoidable nonlinearity in the motion and hence aberrations are introduced due to the curvature of field lines, affecting particles at different locations from reference orbit differently. This method of the DA PDE solver is useful to treat the fringe fields, often the main source of non-deliberate nonlinearities. The process starts with a suitable analytical function describing the field falloff, and a commonly used representation is the Enge function

$$F(s) = \frac{1}{1 + \exp(a_1 + a_2 \cdot (s/D) + \ldots + a_6 \cdot (s/D)^5)}$$

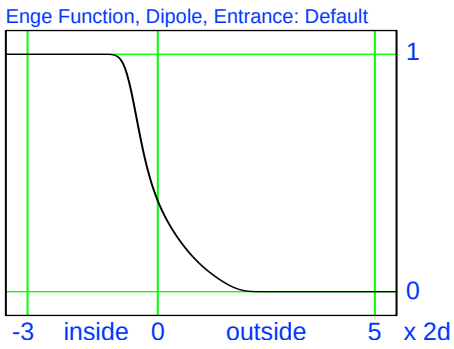

Figure 1. The profile of the default fringe field falloff of electrostatic deflectors and bending magnets.

https://doi.org/10.1017/S1431927615013100 Published online by Cambridge University Press

mode	x_f	a_f	y_f	b_f	l_f	dep.
FR 3	0.876407	-0.024984	0	0	-0.343123	x_i
	9.282307	0.876407	0	0	-1.697380	a_i
	0	0	1.000588	0.000121	0	y_i
	0	0	9.686087	1.000588	0	b_i
	1.697380	0.343123	0	0	1.712180	δ_i
FR 2.5	0.87640**8**	-0.024984	0	0	-0.34312**0**	x_i
	9.282**77**	0.876407	0	0	-1.697**52**	a_i
	0	0	1.000588	0.00012**2**	0	y_i
	0	0	9.686**121**	1.000**90**	0	b_i
	1.697**64**	0.34312**0**	0	0	1.712**64**	δ_i
FR 2.5 Reverse	0.876407	-0.024984	0	0	-0.34312**0**	x_i
	9.282**77**	0.87640**8**	0	0	-1.697**64**	a_i
	0	0	1.000**90**	0.00012**2**	0	y_i
	0	0	9.686**121**	1.000588	0	b_i
	1.697**52**	0.34312**0**	0	0	1.712**64**	δ_i
FR 0	0.876**045**	-0.02**5052**	0	0	-0.343**058**	x_i
	9.2823**48**	0.876**045**	0	0	-1.6973**94**	a_i
	0	0	1.000**000**	0.000**000**	0	y_i
	0	0	9.68**5965**	1.000**000**	0	b_i
	1.6973**94**	0.343**058**	0	0	1.712**239**	δ_i

Table 1. Transfer maps of a cylindrical electric deflector with fringe fields (FR 3, 2.5) and without fringe fields (FR 0). Digits differing from the FR 3 case are marked by bold face. $(l_f|l_i) = 1$ for all cases; omitted to save space.

which has the useful property that the function value smoothly changes from 1 (fully in the main field corresponding to negative s) to 0 (fully outside and sufficiently large positive s). The scalar parameters a_i are chosen suitably, and $D = 2d$ is the full aperture of the device. Figure 1 is an example of an Enge function that is used for bending elements by default both for the electrostatic and the magnetic cases, based on magnet measurement at SLAC. The horizontal axis shows the distance from the effective field boundary in s/D, and the plot is drawn by the FP command in COSY INFINITY [6]. The fields of the entire element now can be obtained via the DA PDE solver by supplying the necessary boundary conditions as the DA multiplication of the s-dependent Enge function and the midplane main field.

An an example to study fringe field effects, we use a cylindrical electrostatic deflector, considered for a storage ring for EDM experiments at Forschungszentrum Jülich, which has an arc length of about 10 m to deflect 22.5° with 24.7 m radius and a half aperture of $d = 5$ cm [12]. The transfer maps of the deflector without and with fringe fields are computed in COSY INFINITY [6], and the linear parts are listed in Table 1. In the field falloff profile seen in Figure 1, the fringe fields span about $3 \cdot D = 6d = 30$ cm in s in both the entrance and the exit of the element, about $1 \cdot D = 10$ cm inside and about $2 \cdot D = 20$ cm outside, a much smaller scale than the entire size of ~ 10 m, resulting in a relatively small discrepancy between the cases without (FR 0) and with (FR 3, FR 2.5) fringe fields. Typically, after establishing an initial design of beam lattices using hard edge elements, the effects of the fringe fields are evaluated, and the system is iteratively tuned based on the findings.

https://doi.org/10.1017/S1431927615013100 Published online by Cambridge University Press

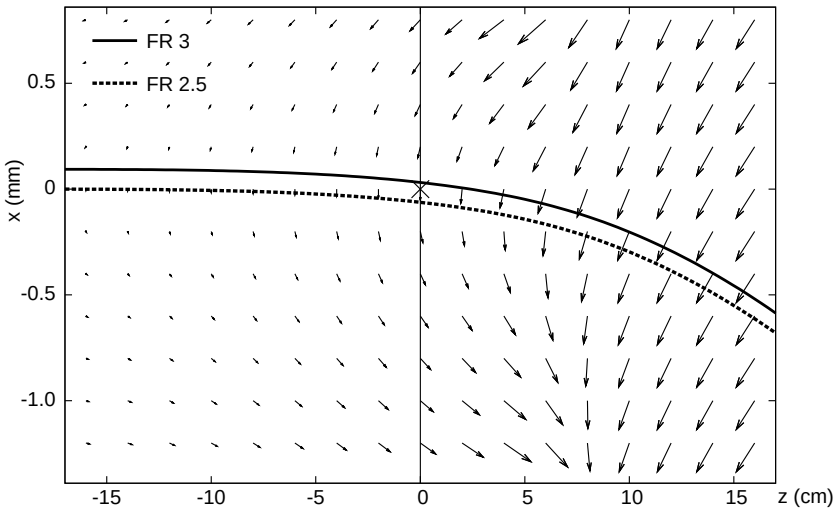

Figure 2. The field distribution of a cylindrical electrostatic deflector and trajectories of the reference particle at the entrance fringe region. E_z is multiplied by 10^4 to emphasize the subtlety of the fringe fields.

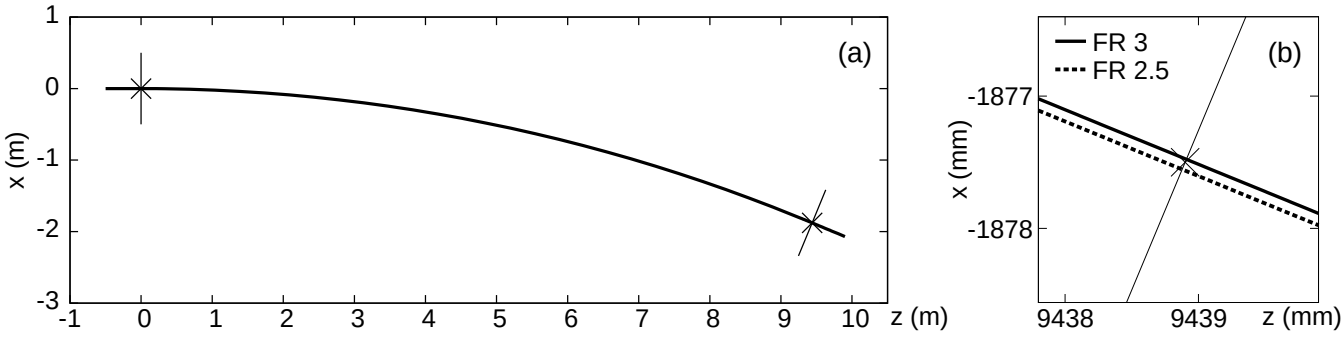

Figure 3. Trajectories of the reference particle in a cylindrical electrostatic deflector. (a) The entire view in the 22.5° deflector with 24.7 m radius, shown in m. (b) The exit area, shown in mm. The effective field boundaries, and the crossing points expected by the hard edge model are marked by lines, and $\times$'s.

Beyond the discrepancies observed in the transfer maps, one encounters the problem that the reference trajectory becomes different from the originally considered ideal one using the hard edge model, which can have far reaching consequences. For the example electrostatic deflector, the horizontal field components (E_z, E_x) in the midplane around the entrance are shown by vectors in Figure 2. For better visualization, the z component E_z is multiplied by 10^4 and also the z and x axis scales differ by a factor of 100. The figure shows the entrance position of the reference orbit in the hard edge mode by a cross, and the actual reference orbits for the fringe field modes FR 3 and FR 2.5 we now discuss.

The fringe field computation mode FR 2.5 calculates the high-order map from $x = 0$ from far left traveling parallel to the z axis. While being the easiest to implement, in this case the reference trajectory throughout the element does not form the expected mirror symmetry about the middle of the element. The linear transfer map of the example electrostatic deflector computed in the mode FR 2.5 is shown in Table 1 together with its reverse map using the command MR to illustrate the difference. In order to enforce the symmetry, it is necessary to first integrate the reference orbit backwards from the middle of the element, and then shift and rotate the element to account for the resulting deviations from the hard edge case. This

https://doi.org/10.1017/S1431927615013100 Published online by Cambridge University Press

x_f	a_f	y_f	b_f	dep.
1	6.696550e-9	0	0	x_i
-6.696550e-9	1	0	0	a_i
0	0	1	-4.702209e-15	y_i
0	0	4.702209e-15	1	b_i
-3.061968e-12	-6.688603e-16	0	0	x_i^2
-1.339527e-8	4.364584e-16	0	0	$x_i a_i$
...	...	...	...	...
0	0	2.084504e-8	-4.517182e-5	b_i^5

Table 2. A transfer map of a non-relativistic spherical electrostatic deflector of 360°.

x_f	a_f	y_f	b_f	deep.
0.786219	-0.686056	0	0	x_i
0.556601	0.786219	0	0	a_i
0	0	1	0	y_i
0	0	0.600000	1	b_i
0	0	-1	0	$\triangle_y$
-0.357515	0.072130	0	0	x_i^2
...	...	...	...	...
-0.173442	-0.556601	0	0	b_i^2
...	...	...	...	...
0	0	0.130739	0	b_i^5

Table 3. A transfer map of a cylindrical electrostatic deflector followed by a vertical position offset, $\mathscr{M}_{\triangle y} \circ \mathscr{M}_{cl}$, which agrees with $\mathscr{M}_{cl} \circ \mathscr{M}_{\triangle y}$.

is done in the mode FR 3, and the obtained linear transfer map is listed in Table 1 as well. In this case, the reversed map via MR agrees with the forward map as it should, and the starting x position at far left is shifted accordingly; in the example element, ~ 0.1 mm offset is turned out. The reference trajectories of the both cases are plotted in Figures 2 and 3.

Besides the problem of the trajectory offset that needs to be accounted for, there is another major problem since particle optical elements with fringe fields are usually described by three separate parts, namely the entrance fringe field, the main field, and the exit fringe fields. But in electrostatic elements, at the end of the entrance fringe fields there are nonzero potentials affecting the particle's energy. If this is now followed by a shift or rotation of the reference orbit to line up with the subsequent main field, as is usually done, this leads to a jump of potential and a violation of energy conservation. While seemingly small, these effects can very detrimentally build up in repetitive systems as seen in Figure 4. Thus different from common particle optical practice, the above discussed fringe field computation modes, FR 3 and FR 2.5, in COSY INFINITY carry the computation throughout the entire element including the entrance and exit fringe field regions.

We now describe some consistency tests and observations for electrostatic deflectors that allow far-reaching cross checks of high-order aberrations. The first test is based on the observation that the motion is that of a Kepler problem, which entails that in the non-relativistic case the motion should return to the exact

https://doi.org/10.1017/S1431927615013100 Published online by Cambridge University Press

x_f	a_f	y_f	b_f	dep.
0.055684	-0.481518	0	0	x_i
2.070327	0.055684	0	0	a_i
0	0	-1	-3.043659e-16	y_i
0	0	3.043659e-16	-1	b_i
0	0	2.220446e-16	3.043659e-16	$\triangle$
-0.996899	3.313187e-16	0	0	x_i^2
...	...	...	...	...
2.070327	-0.944316	0	0	$y_i b_i$
0.524939	-0.225147	0	0	x_i^3
...	...	...	...	...
0	0	-1.157618e-11	-4.060167	$y_i^2 b_i^3$

Table 4. A transfer map a spherical electrostatic deflector of 180° with tilts of plane $\mathscr{M}_{\triangle} \circ \mathscr{M}_{sp180} \circ \mathscr{M}_{\triangle}$.

original state after one full revolution, independent of initial conditions. Thus a transfer map of a spherical deflector of 360° should be an identity map. For the test, the fringe fields must not be included. The short code in COSY INFINITY

```
OV 5 2 0 ; RPP 1e-6 ; UM ; ESP 1 360 0.1 ; PM 6 ;
```

computes such a map up to the fifth order, and part of the resulting output omitting lengthy intermediate terms is listed in Table 2, demonstrating the intended result. A "lattice" consisting of n spherical deflectors of angle $360^\circ/n$ also produces the same result.

The second test is to demonstrate that the motion in an electrostatic cylindrical deflector is invariant under translation along the y axis, and the y motion behaves like a drift. Furthermore, although the x motion depends on y and b, an offset in the y direction does not alter the x motion. Thus, a transfer map of a cylindrical deflector $\mathscr{M}_{cl}$ and a y offset map $\mathscr{M}_{\triangle y}$ need to commute; i.e., $\mathscr{M}_{cl} \circ \mathscr{M}_{\triangle y} = \mathscr{M}_{\triangle y} \circ \mathscr{M}_{cl}$. For the test, we express the offset Δ_y as a DA parameter, and the displacement map $\mathscr{M}_{\triangle y}$ can be produced by an axis offsetting command SA in COSY INFINITY with `DA(5)` for the y offset. The displacement map $\mathscr{M}_{\triangle y}$ has $(y|\triangle_y) = -1$ added into the identity map, and is listed in Table 5. The next short code computes $\mathscr{M}_{\triangle y} \circ \mathscr{M}_{cl}$ up to the 5th order.

```
OV 5 2 1 ; RP 1000 1 1 ; UM ; ECL 1 PHI 0.08 ; SA 0 DA(5) ; PM 6 ;
```

And the next one computes $\mathscr{M}_{cl} \circ \mathscr{M}_{\triangle y}$ up to the 5th order.

```
OV 5 2 1 ; RP 1000 1 1 ; UM ; SA 0 DA(5) ; ECL 1 PHI 0.08 ; PM 6 ;
```

Here the deflection angle `PHI` is insignificant, and for the purpose of the computation we choose `PHI := 0.6*180/PI ;` which amounts to about 34.36°. The resulting output showing some selected aberrations is listed in Table 3. The two resulting transfer maps agree up to the accuracy of 10^{-14}, succeeding the test. It is worth noting that the deflector transfer map $\mathscr{M}_{cl}$ is the same as the one in Table 3 except for missing the Δ_y dependent term in the 5th line.

A similar displacement test can be performed for an electrostatic spherical deflector, as it has to be invariant under any rotation around an axis through the center. This test involves a tilt of the plane of motion through the deflector along a central axis parallel to the reference orbit. Such a tilt of plane consists of a series of misalignment actions in the optical system; first translate the system in the x direction to the spherical center for the amount of radius `R`, next rotate the system any angle θ, then translate the system back to the

https://doi.org/10.1017/S1431927615013100 Published online by Cambridge University Press

coef.	$\mathscr{M}_{\triangle y}$	$\mathscr{M}_{\triangle}$	comment
1	$(x\|x)$, $(a\|a)$, $(y\|y)$, $(b\|b)$		identity
-1	$(y\|\triangle_y)$	$(y\|\triangle)$, $(y\|x\triangle)$, $(b\|a\triangle)$	
1		$(x\|y\triangle)$, $(a\|b\triangle)$	
-0.500000		$(x\|\triangle^2)$, $(x\|x\triangle^2)$, $(a\|a\triangle^2)$, $(y\|y\triangle^2)$, $(b\|b\triangle^2)$	0.500000=1/2!
0.166667		$(y\|\triangle^3)$, $(y\|x\triangle^3)$, $(b\|a\triangle^3)$	0.166667=1/3!
-0.166667		$(x\|y\triangle^3)$, $(a\|b\triangle^3)$	
0.041667		$(x\|\triangle^4)$, $(x\|x\triangle^4)$, $(a\|a\triangle^4)$, $(y\|y\triangle^4)$, $(b\|b\triangle^4)$	0.041667=1/4!

Table 5. Transfer maps of the vertical offset $\mathscr{M}_{\triangle y}$, and the tilt of plane $\mathscr{M}_{\triangle}$.

sphere of the same radius R. This corresponds to a move from the equator to the north on the same longitude to the location with the latitude of θ. A corresponding map of plane tilting $\mathscr{M}_{\triangle}$ can be achieved using the axis offset command SA and the axis rotation command RA in COSY INFINITY by the following code

```
SA -R 0 ; RA DA(5) ; SA R 0 ;
```

where we are setting the tilt angle as a DA parameter. Now choosing a spherical deflector with a deflection of 180° entails that the reference orbit after the deflection is parallel to the reference orbit before the deflection, but points in the opposite direction. Indeed, for the purpose of matching a move of a 180° deflection on the equator, one first moves northward to latitude θ , then travels for 180° around the center to arrive opposite to the starting location and thus at latitude $-\theta$, and then has to move back north by the angle $+\theta$ to reach the equator. So, a transfer map of the deflection combined with two tilts of plane $\mathscr{M}_{\triangle} \circ \mathscr{M}_{sp180} \circ \mathscr{M}_{\triangle}$, must agree with the transfer map of the deflection alone $\mathscr{M}_{sp180}$. We compute $\mathscr{M}_{sp180}$ up to the 5th order by the code

```
OV 5 2 1 ; RP 1000 1 1 ; UM ; ESP 1 180 0.1 ; PM 6 ;
```

While $\mathscr{M}_{\triangle} \circ \mathscr{M}_{sp180} \circ \mathscr{M}_{\triangle}$ can be computed by the code

```
PROCEDURE RRA R T ; SA -R 0 ; RA T*DA(5) ; SA R 0 ; ENDPROCEDURE ;
OV 5 2 1 ; RP 1000 1 1 ; UM ; RRA 1 T ; ESP 1 180 0.1 ; RRA 1 T ; PM 6 ;
```

Since the RA command expects angles in degrees, `T := 180/PI ;` is supplied to obtain the output of $\mathscr{M}_{\triangle}$ in terms of radian, which is listed in Table 5. Similarly the result of computing $\mathscr{M}_{\triangle} \circ \mathscr{M}_{sp180} \circ \mathscr{M}_{\triangle}$ is listed in Table 4, again omitting lengthy intermediate terms and observing that Δ dependent terms are negligible. Apparently this 5th order map agrees with $\mathscr{M}_{sp180}$ up to an accuracy of 10^{-9}, as it should from the theoretical discussion.

To assess the discussed methods in practical settings, we perform long term nonlinear tracking. Using an earlier studied example of the electrostatic cylindrical deflector of 22.5° deflection, 24.7 m radius and half aperture $d = 5$ cm, we set up a very simple cell by adding a drift of 0.6 m. We compare various computation orders up to seven and the fringe field computation modes FR 0, FR 2.5, FR 3, and the classical piece-by-piece computation mode frequently used in particle optics. Particles are launched at $x = 5$ mm, 10 mm, 15 mm and 20 mm, the 6D positions are tracked and we plot the phase space position in the *x*-*a* plane for every revolution consisting of 16 cells for 5000 turns.

The resulting FR 0 motion with no fringe field is stable and looks the same throughout the studied computation orders; the 7th order case is shown in Figure 4 (a). When fringe fields are considered, the situation gets interesting. Both modes FR 3 and FR 2.5 provide stable motion for all orders computed, and the *x*-*a* plots look indistinguishable from the FR 0 case; the 7th order case with FR 3 is shown in Figure 4 (d). In

https://doi.org/10.1017/S1431927615013100 Published online by Cambridge University Press

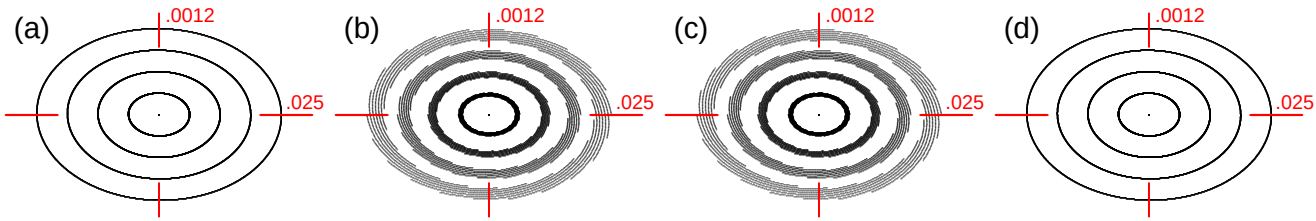

Figure 4. Long term tracking of an electrostatic cylindrical deflector, comparing various fringe field modes (a: FR 0. b, c: piece-by-piece mode. d: FR 3) and the computation orders (a, b, d: 7th. c: 3rd).

the piece-by-piece computation method to treat the fringe fields, we expect to observe some violations of the energy conservation. Indeed when performing long term tracking, we observe it in (b) for the order 7 case and in (c) for order 3 in 4. No difference is visible between (b) and (c), and so we conclude that the observed effects are due to the energy mismatch in the piece-by-piece computation, the bulk of which already manifests itself in low orders and which is not remedied by using higher orders.

From basic principles of charged particle motions, our discussion started from distinct properties of the electrostatic and the magnetic elements for the purpose of bending charged beams. Based on the Differential Algebraic (DA) method, efficient techniques to compute high order transfer maps, the necessary 3D fields including the edge region, and the effects of fringe fields are discussed. They are illustrated using both benchmarks for cross checking as well as long term repetitive tracking examples that exhibit various difficulties that can arise in practice [13].

References:

[1] Storage Ring Electric Dipole Moment Collaboration, http://www.bnl.gov/edm/. JEDI (Jülich Electric Dipole Moment Investigations) Collaboration, http://collaborations.fz-juelich.de/ikp/jedi/.
[2] A Lehrach, Proceedings of ICAP2012, Rostock-Warnemünde (2012) p. 7.
[3] M Berz, K Makino and W Wan, “An introduction to beam physics”, (Taylor & Francis, London, 2014).
[4] M Berz, “Modern map methods in particle beam physics”, (Academic Press, San Diego, 1999).
[5] K Makino, M Berz and C Johnstone, International Journal of Modern Physics A **26** (2011), p. 1807.
[6] M Berz and K Makino, “COSY INFINITY version 9.1 beam physics manual”, MSUHEP-060804-rev, (Michigan State University, East Lansing, 2013), http://cosyinfinity.org.
[7] R Hipple and M Berz, in these proceedings.
[8] B Erdélyi and M Berz, Physical Review Letters **87** (2001), p. 114302.
[9] K Makino, “Rigorous analysis of nonlinear motion in particle accelerators”, PhD thesis, (Michigan State University, East Lansing, 1998).
[10] M Berz and K Makino, International Journal of Applied Mathematics **3** (2000), p. 401.
[11] K Makino and M Berz, International Journal of Applied Mathematics **3** (2000), p. 421.
[12] D Zyuzin, private communication.
[13] We are grateful for financial support from the US Department of Energy under grant DE-FG02-08ER41546.

https://doi.org/10.1017/S1431927615013100 Published online by Cambridge University Press